

Fiber Stretch and Reorientation Modulates Mesenchymal Stem Cell Morphology and Fibrous Gene Expression on Oriented Nanofibrous Microenvironments

SU-JIN HEO,¹ NANDAN L. NERURKAR,¹ BRENDON M. BAKER,^{1,3} JUNG-WOOG SHIN,² DAWN M. ELLIOTT,^{1,3}
and ROBERT L. MAUCK^{1,3}

¹McKay Orthopaedic Research Laboratory, Department of Orthopaedic Surgery, University of Pennsylvania, 424 Stemmler Hall, 36th Street and Hamilton Walk, Philadelphia, PA 19104-6081, USA; ²Department of Biomedical Engineering, Inje University, Gimhae, Republic of Korea; and ³Department of Bioengineering, University of Pennsylvania, Philadelphia, PA 19104, USA

(Received 9 May 2011; accepted 18 July 2011)

Associate Editor Michael S. Detamore oversaw the review of this article.

Abstract—Because differentiation of mesenchymal stem cells (MSCs) is enacted through the integration of soluble signaling factors and physical cues, including substrate architecture and exogenous mechanical stimulation, it is important to understand how micropatterned biomaterials may be optimized to enhance differentiation for the formation of functional soft tissues. In this work, macroscopic strain applied to MSCs in an aligned nanofibrous microenvironment elicited cellular and nuclear deformations that varied depending on scaffold orientation. Reorientation of aligned, oriented MSCs corresponded at the microscopic scale with the affine approximation of their deformation based on macroscopic strains. Moreover, deformations at the subcellular scale corresponded with scaffold orientation, with changes in nuclear shape depending on the direction of substrate alignment. Notably, these deformations induced changes in gene expression that were also dependent on scaffold and cell orientations. These findings demonstrate that directional biases in substrate microstructure convey direction-dependent mechanosensitivity to MSCs and provide an experimental framework in which to explore the mechanistic underpinnings of this response.

Keywords—Mechanobiology, Electrospinning, Biomaterials, Microenvironment.

INTRODUCTION

In order to function *in vivo*, many musculoskeletal soft tissues contain an extracellular matrix (ECM), consisting of ordered arrays of collagen which in turn creates structural and mechanical anisotropy.²⁷ Engineering successful replacements for these tissues will likely require replication of this ordered fibrous architecture. One polymer processing technique, electrospinning, permits the fabrication of mechanically anisotropic scaffolds composed of aligned arrays of nanofibers that support cell survival, migration, and differentiation.²³ Electrospun nanofibers orient cells and direct ECM deposition, making them particularly promising for engineering tissues with well defined micro-architectures, including tendon,^{26,43} the knee meniscus,¹⁻³ and the annulus fibrosus of the intervertebral disc.^{31,33,34,44} These scaffolds also provide a template for studying mechanobiology in the context of changing topographical cues from the microenvironment.

Mesenchymal stem cells (MSCs) are a clinically appealing cell source for tissue engineering due to their multi-potentiality and ease of harvest.³⁷ However, functional differentiation of MSCs remains a challenge, particularly when induction protocols rely solely on chemical mediators. This is perhaps best illustrated in cartilage tissue engineering, where induction of cartilage molecular markers by MSCs can be readily achieved in the presence of certain growth factors, while long-term mechanical function remains inferior to chondrocytes cultured and maintained similarly.^{16,24}

Address correspondence to Robert L. Mauck, McKay Orthopaedic Research Laboratory, Department of Orthopaedic Surgery, University of Pennsylvania, 424 Stemmler Hall, 36th Street and Hamilton Walk, Philadelphia, PA 19104-6081, USA. Electronic mail: lemauck@mail.med.upenn.edu

Indeed, many recent studies suggest that, in addition to soluble cues, MSC phenotypic transitions are influenced by physical cues arising from the microenvironment, including substrate surface chemistry,^{8,12,36} cell shape,²⁵ and substrate elasticity.¹⁴ For example, we have recently shown that MSCs in pellet culture (rounded morphology) express higher levels of chondrogenic markers compared with MSCs seeded onto an aligned nanofibrous topography (elongated morphology), where fibrous markers predominate.² Effective use of MSCs for tissue engineering requires an improved understanding of how soluble molecular signals are integrated with microenvironmental inputs to inform lineage commitment.

In addition to these passive inputs from the microenvironment, long-term mechanical perturbation, applied through deformational bioreactors, can enhance functional differentiation of MSCs both in hydrogels (in compression)¹⁵ and on nanofibrous scaffolds (in tension).⁵ The subcellular mechanisms that relate such forces to changes in gene expression are unclear. Nuclear morphology is thought to be a determinant of transcriptional activity, as deformation of the nucleus involves mechanical reorganization of chromatin, potentially making certain genes more or less accessible to transcription factors.^{11,19,40,42} For nanofibrous networks, scaffold alignment directs a baseline deformation of the nucleus into an elliptical shape, where the long axis is closely aligned with the underlying nanofibers.²⁸ This is likely due to cell-generated traction forces associated with the elongation and adhesion of cells to the scaffold. Step-wise tensile strain of scaffolds applied parallel to the direction of fiber alignment results in step-wise increases in nuclear deformation in resident MSCs.²⁸ These extracellular deformations are translated to the nucleus through the actin cytoskeleton. When similar magnitudes of tensile strain are applied perpendicular to the fiber direction, little change in cell or nuclear morphology occurs.²⁸ These findings suggest that modulation of nuclear shape by externally applied strain involves the superposition of nuclear shape changes onto those dictated by scaffold topography.

For some tissues, interpreting the subcellular physical cues that arise from macroscopic deformation requires additional considerations at the microstructural level. The annulus fibrosus of the intervertebral disc, for example, is an angle-ply laminate, with alternating lamellae of locally aligned collagen bundles oriented above and below the circumferential axis of the spine. The ply angles change radially across the disc, with the outer annulus having a $\pm 30^\circ$ orientation and the inner annulus having a $\pm 45^\circ$ orientation.²² Nanofibrous scaffolds with a single, aligned fiber population—and tissues generated from seeding these

scaffolds with cells—exhibit a large reduction in tensile modulus when the direction of strain deviates from the direction of cell and nanofiber alignment by 30° or greater.^{30,31} This observation has implications for mechanically guided maturation of engineered annulus fibrosus constructs: in multi-ply annulus fibrosus laminates,²⁹ application of tensile strain would yield differing effects on cells in scaffolds composed of different ply angles.

Understanding the role of fiber architecture as it pertains to cell and nuclear deformations has important implications for tissue engineering in the context of a mechano-active cellular environment. Despite progress to date, it remains unclear how scaffold microstructure influences the transmission of extracellular deformations to the nucleus, particularly for the special case where scaffold alignment does not coincide with the macroscopic direction of strain. While it is often assumed that cells experience local strains similar to those applied macroscopically, this is not the case for materials with defined aligned and oriented microarchitectures. Therefore, the objective of this work was to examine how changes in scaffold fiber orientation influence cellular and subcellular deformation of MSCs on electrospun scaffolds subjected to static tensile strain (Fig. 1). By altering the direction of cell alignment with respect to the direction of strain, it is possible to modulate local deformations such that uniaxial strain at the tissue-level can be translated to varying degrees of strain, shear, and compression at the cellular and subcellular length scale (Fig. 1). Using this precise control of microenvironment, we sought to investigate how such variations in local kinematics (fiber stretch and reorientation) with scaffold orientation influence the transcriptional response of MSCs exposed to macroscopic tensile strain.

MATERIALS AND METHODS

Fabrication of Aligned Nanofibrous Scaffolds

Poly(ϵ -caprolactone) (PCL, mol. wt. 80 kDa, Shenzhen Bright China Industrial Co., Ltd., China) nanofibers were formed by electrospinning as described previously.^{1,29} Briefly, 4 g of PCL was dissolved in 28 mL of equal parts tetrahydrofuran and *N,N*-dimethylformamide (Fisher Scientific, Pittsburgh, PA). The mixture was loaded into a syringe with an 18G stainless steel needle serving as a spinneret. PCL was ejected at a rate of 2.5 mL h⁻¹ through the spinneret, which was charged to 13 kV (ES30P-5W; Gamma High Voltage Research Inc., Ormand Beach, FL). To instill alignment, nanofibers were collected on a mandrel rotating with linear velocity 10 m s⁻¹,

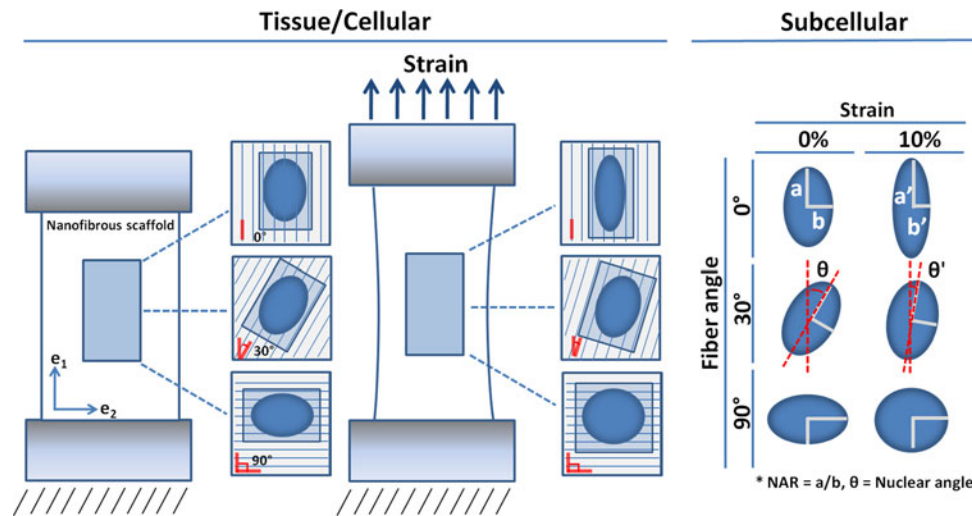


FIGURE 1. Schematic illustrating the differential effects of initial scaffold nanofiber alignment on deformation at the cellular and subcellular scales following application of macroscopic/tissue-level uniaxial tensile strain (a/b = undeformed major/minor ellipsoidal axes, a'/b' = deformed major/minor ellipsoidal axes; NAR = nuclear aspect ratio; θ/θ' = nuclear orientation in the undeformed/deformed configuration).

distanced 15 cm from the spinneret. Scaffolds were excised from the resulting nanofibrous mat ($5 \times 60 \times \sim 0.70 \text{ mm}^3$) with the long axis of the construct rotated from the direction of fiber alignment by angles of $\theta = 0^\circ, 15^\circ, 30^\circ, 45^\circ,$ and 90° .³⁰ Scaffolds were sterilized and rehydrated by incubating in decreasing concentrations of ethanol (100, 70, 50, 30, 0%; 30 min/step). Additional samples were subjected to scanning electron microscopy to visualize nanofiber morphology as described previously.¹

Mechanical Testing of Scaffolds

Mechanical properties of electrospun nanofibrous scaffolds were evaluated by tensile testing ($n = 7$ per orientation) using an Instron 5848 Microtester (50 N load cell, Instron, Canton, MA). The thickness of each scaffold was measured using a custom non-contacting laser-based system.³⁵ Scaffold gauge length was determined via digital calipers after placement in serrated grips. Scaffolds were pre-conditioned with 10 cycles of sinusoidal loading to 0.1 N at a frequency of 0.1 Hz. Subsequently, scaffolds were extended to failure at a rate of $0.1\% \text{ s}^{-1}$. Stress was computed as the force divided by initial cross sectional area, and longitudinal/applied strain (E_1) was computed by dividing displacement by the initial gauge length. Tensile modulus was calculated by regression to the linear region of the stress-strain plot. To calculate Poisson's ratio, images of the scaffold mid-substance ($n = 5/\text{group}$) were captured at a rate of 0.5 Hz throughout the tensile test. At 5 and 10% grip-to-grip strain, images were analyzed in Image J to determine change in width, which was divided by initial width to

compute transverse strain (E_2). Poisson's ratio (ν) was computed at 5 and 10% strain as the ratio $\nu = -E_2/E_1$.

Cell and Nuclear Visualization with Applied Strain

MSCs were isolated from juvenile bovine bone marrow (Research 87, Inc., Boylston, MA) as in Mauck *et al.*²⁴ and expanded through passage 2 in basal medium (Dulbecco's modified Eagle's medium containing 10% fetal bovine serum and 1% penicillin, streptomycin, and fungizone). Scaffolds were incubated in $20 \mu\text{g mL}^{-1}$ fibronectin in PBS for 12 h, then seeded with MSCs by delivering 100 μL of a concentrated cell solution to the scaffold surface to achieve a seeding density of 250 cells per mm^2 .²⁸ Scaffolds ($5 \times 60 \times \sim 0.70 \text{ mm}^3$, $n = 3$) were then incubated for 1 h at 37°C to allow for attachment prior to the addition of basal medium.

After 24 h of further incubation, cell-seeded scaffolds were subjected to static tensile strain using a custom loading device described previously.²⁸ Briefly, the device permits application of defined strain to constructs, while allowing visualization of the scaffold surface via fluorescence microscopy. Constructs were strained at $2.5\% \text{ strain min}^{-1}$ to 10% total grip-to-grip strain. At 0, 5, and 10% grip-to-grip strain, constructs were fixed with 4% paraformaldehyde at 37°C for 20 min, and washed three times in PBS.²⁸ To visualize the actin cytoskeleton, cells were permeabilized with 1% Triton X-100 for 5 min and stained with phalloidin-Alexa488 (Invitrogen, Carlsbad, CA) as in Li *et al.*²⁰ Nuclei were counter-stained with 4',6-diamidino-2-phenylindole (DAPI). All images were captured on an inverted fluorescent microscope (Nikon

T30, Nikon Instruments, Melville, NY) equipped with a CCD camera.²⁸

Measurement and Prediction of Cell and Nuclear Reorientation

At each applied strain, the orientation of cells and nuclei ($n = 98$ from three different samples) with respect to the loading direction and the nuclear aspect ratio (ratio of nuclear long axis to short axis, NAR) ($n = 50$ from three different samples) were determined from fluorescent images using Image J (Fig. 1).²⁸ These measures were compared with global deformations to determine whether local cellular and subcellular deformations occur in an affine manner. This was accomplished by constructing a deformation gradient tensor, \mathbf{F} , associated with each deformation state. \mathbf{F} was defined in a Cartesian coordinate system where x_1 defines the direction of loading and all fibers lie within the x_1 - x_2 plane. The matrix form of \mathbf{F} was defined as:

$$[\mathbf{F}] = \begin{bmatrix} \lambda_1 & 0 & 0 \\ 0 & \lambda_2 & 0 \\ 0 & 0 & \lambda_3 \end{bmatrix}$$

where λ_i are the stretch ratios along each direction $i = 1, 2, 3$. For each simulation, a state of plane strain was assumed ($\lambda_3 = 1$), λ_1 was varied from 1 to 1.1 (corresponding to 10% tensile strain), and λ_2 was determined from λ_1 according to Poisson's ratio measured above for acellular scaffolds. Because \mathbf{F} maps line elements within a continuum from their undeformed to deformed state, it was assumed that cells and nuclei could be approximated as such. Deformations were approximated according to the equation:

$$\vec{dr} = \mathbf{F} \vec{dR}$$

where \vec{dr} and \vec{dR} represent a material line element in the deformed and undeformed configuration, respectively.

Gene Expression

Changes in the expression of fibrous markers were determined by real time RT-PCR to assess the phenotypic consequences of applied static tensile strain as a function of nanofiber orientation. At 0.5, 1, and 3 h after application of strain, samples ($5 \times 60 \times \sim 0.70$ mm³, $n = 3$) were immediately frozen in Trizol, and mRNA was isolated by phenol-chloroform extraction. RNA concentration was quantified (ND-1000, Nanodrop Technologies, Wilmington, DE, USA) and cDNA synthesized using the SuperScript First Strand Synthesis kit (Invitrogen Life Technologies, Carlsbad, CA). Amplification was performed with gene specific primers using

an Applied Biosystems 7300 real time PCR system with the SYBR Green Reaction Mix (Applied Biosystems, Foster City, CA, USA). Expression levels of collagen type I (COL-I, 5'-AATTCCAAGGCCAAGAAGCATG-3' and 3'-GGTAGCCATTTCTTGGTGGTT-5'), tenascin C (TNC, 5'-TGCCCATTGCAGGAGGTGCG-3' and 3'-GGGCGATGACGCTGACCAGG-5'), and lysyl oxidase (LOX, 5'-GGAACACTACATCCTCAAGGTGCAT-3' and 3'-CGACATTGTTGGTGAAGTCAGACT-5') were determined and normalized to the housekeeping gene glyceraldehyde-3-phosphate dehydrogenase (GAPDH, 5'-ATCAAGAAGGTGGTGAAGCAGG-3' and 3'-TGAGTGTGCTGTTGAAGTCG-5').

Statistical Analyses

Statistical analyses were performed by two-way analysis of variance (ANOVA) with Bonferroni *post hoc* tests to make comparisons between groups (SYSTAT v. 10.2, Point Richmond, CA, USA). All results are expressed as the mean \pm standard deviation. Differences were considered statistically significant at $p < 0.05$.

RESULTS

Fabrication and Mechanical Testing of Aligned Nanofibrous Scaffolds

Nanofibrous poly(ϵ -caprolactone) PCL scaffolds were fabricated with highly aligned fibers of ~ 700 nm diameter (Fig. 2a). Within 24 h of seeding, adherent MSCs were observed with prominent stress fibers oriented parallel to the fiber direction (Fig. 2b, c). To determine how directional biases in microstructural alignment affect mechanotransduction of MSCs, the macroscopic mechanical properties of electrospun nanofibrous PCL mats were first examined by uniaxial tensile testing. Consistent with previous results,³⁰ tensile moduli decreased nonlinearly as fiber angle increased with respect to the direction of applied deformation (Fig. 2d). Poisson's ratio (the ratio of lateral to longitudinal strain) varied significantly with fiber angle (Fig. 2e). Poisson's ratio decreased monotonically for scaffolds with orientations greater than 15° ($p < 0.01$).

Cell and Nuclear Reorientation with Applied Strain

To determine how these variations in macroscopic mechanical properties relate to cell and subcellular deformation, uniaxial strain was applied to MSC-seeded scaffolds at each fiber orientation (Figs. 1, 3a). Cellular and nuclear orientations were measured to

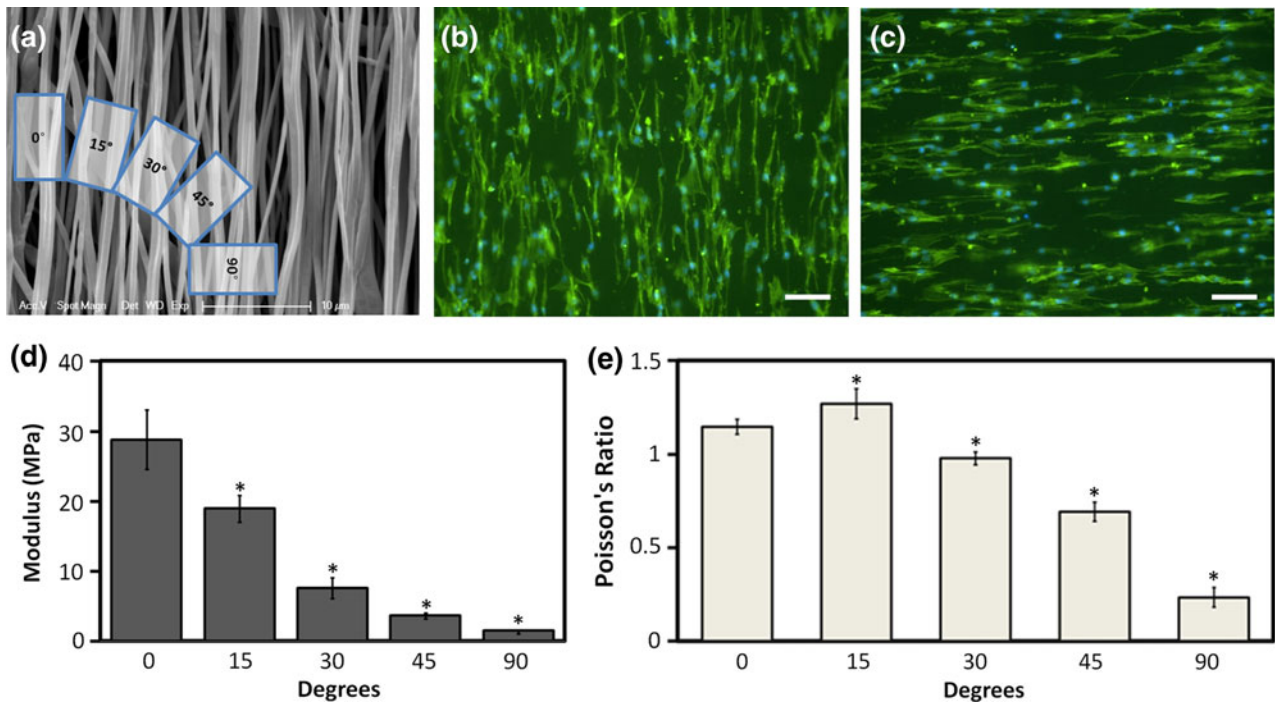


FIGURE 2. Aligned nanofibrous scaffolds were prepared with a range of fiber orientations with respect to the scaffold long axis (scale bar = 10 μm). Shown in (a) is a schematic illustration of how scaffolds are excised from an aligned fibrous mat to produce individual scaffolds whose internal fiber alignment is not coincident with the long axis over which tensile deformation is applied. MSCs seeded on 0° and 90° scaffolds were highly aligned and followed the fiber direction (b and c; blue (DAPI) and green (phalloidin) indicate nucleus and actin, respectively; scale bar = 100 μm). Tensile modulus decreased nonlinearly as fiber angle increased (d; $n = 7$, $*p < 0.01$ vs. 0° scaffold). Poisson's ratio varied significantly with alterations in fiber direction and strain (e; $n = 5$, $*p < 0.05$ vs. 0°). Data represent the mean \pm SD.

determine whether local cellular reorientation occurs affinely, and to determine to what extent macroscopic strain dictates nuclear rotation as the direction of local substrate alignment was varied. The initial/undeformed MSC orientation (in degrees) with respect to the long axis (i.e., loading direction) of the scaffold were 14.1 ± 3.2 (for 15° scaffolds), 29.1 ± 3.6 (for 30° scaffolds), and 44.4 ± 3.7 (for 45° scaffolds) (Figs. 3, 4). Nuclei were also oriented along the scaffold fiber direction, but with less fidelity than cell bodies (15°: 23.7 ± 6.2 , 30°: 38.4 ± 5.0 , 45°: 57.0 ± 6.4 ; Fig. 4). With tensile deformation of the scaffold, MSCs progressively rotated toward the direction of applied strain (Figs. 3, 4). With 5% strain, a reduction in cell orientation angle ($n = 98$, $p < 0.05$) was observed for all scaffolds except 15° scaffolds, while nuclear orientations did not decrease for any scaffold orientation ($p > 0.05$). With 10% strain, both cells and nuclei rotated towards the strain direction compared to the unstrained state. At 10% strain, cell orientations were 15°: 10.8 ± 2.6 , 30°: 20.0 ± 5.3 , 45°: 35.9 ± 5.2 , while nuclear orientations were 15°: 16.3 ± 4.3 , 30°: 29.5 ± 5.2 , 45°: 51.0 ± 6.2 ($n = 98$, $p < 0.01$ vs. all measured 0% strain values).

Predictions of affine fiber/cell rotations were computed with the assumption that fibers deform as

material line elements in a continuum. At 5% strain, predicted values for fiber orientations were 15°: 13.8 ± 0.9 , 30°: 27.4 ± 0.9 , 45°: 42.8 ± 0.9 . At 10% strain, predicted values were 15°: 11.8 ± 0.8 , 30°: 25.8 ± 0.8 , 45°: 40.1 ± 0.9 ($n = 3$). Direct measure of cell reorientation in each of the 15°, 30°, and 45° scaffolds agreed well with the theoretical predictions (i.e., measured values were not significantly different from the predicted value, $p > 0.05$), except for 30° scaffolds at 10% strain (Fig. 4, closed circles) where cell reorientation occurred to a slightly greater extent than was predicted. Unlike cells, nuclear reorientation did not follow this affine prediction, particularly at lower strains (Fig. 4, open circles, $p < 0.05$ vs. predicted values at every orientation and strain magnitude).

Nuclear Aspect Ratio with Applied Strain

Next, the nuclear aspect ratio (NAR) was determined to quantify changes in nuclear shape with increasing strain for each fiber orientation. NAR was greater than one in the undeformed state (NAR: 1.74 ± 0.21) (Fig. 5).²⁸ When the direction of strain coincided with or was close to the fiber direction (i.e., 0° and 15° scaffolds), NAR did not change with 5% strain, but increased significantly with 10% strain

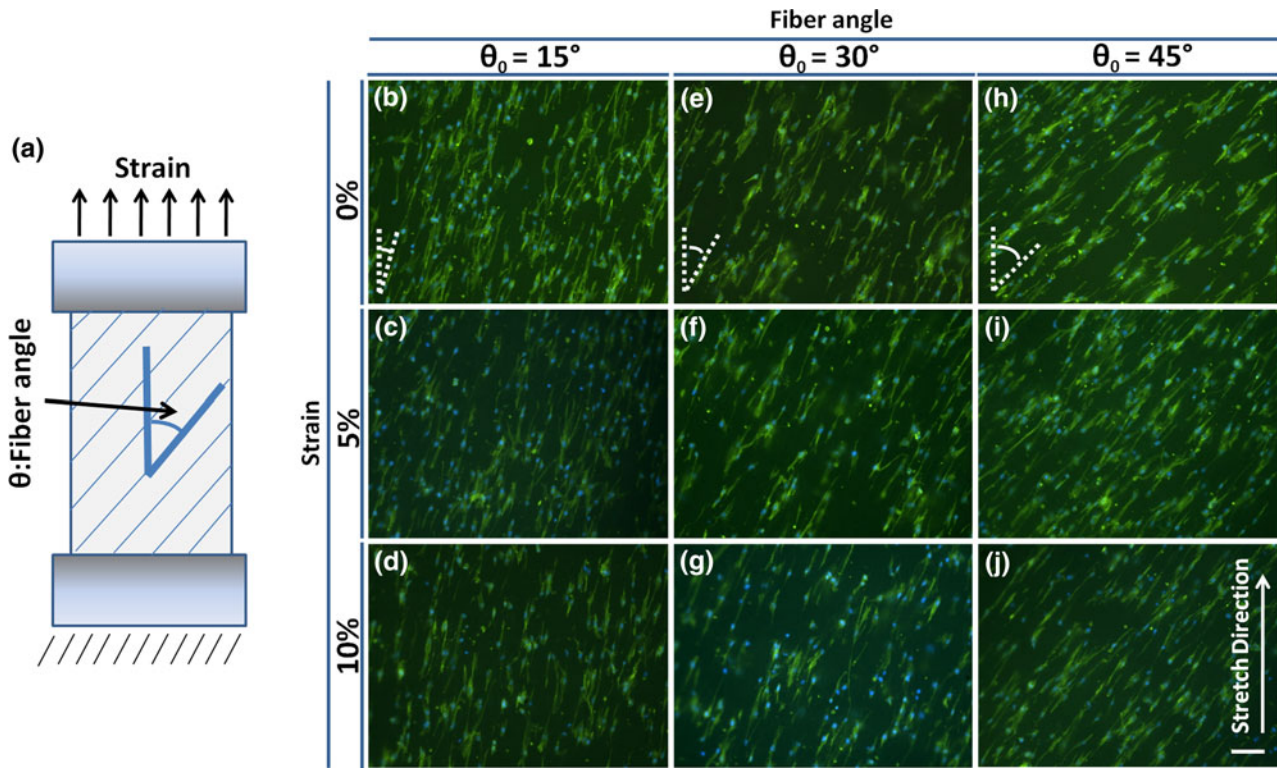


FIGURE 3. Schematic illustrating stretch direction for scaffolds with varying fiber angles (a). MSCs were highly oriented on aligned scaffolds with prominent actin stress fibers (green, phalloidin) extending along the fiber direction (b, e, and h). Cells rotated toward the stretch direction with increasing tensile strain (5% strain: c, f, and i; 10% strain: d, g, and j; scale bar = 100 μm).

(0° : 2.10 ± 0.22 , $p < 0.01$; 15° : 1.94 ± 0.16 , $p < 0.05$). Conversely, NAR decreased when 10% strain was applied perpendicular to the fiber direction (90° : 1.60 ± 0.11 , $p < 0.05$). For scaffolds with fiber angles intermediate to these two extremes, no significant change in NAR was observed (Fig. 5).

Anisotropic Changes in Gene Expression with Tensile Strain

To determine whether these variations in cellular and subcellular deformations with local substrate directionality correspond to alterations in mechanotransduction, changes in gene expression with macroscopic strain were next examined. Prolonged exposure to static tensile strain resulted in dynamic changes in the expression of fibrous markers that were dependent on fiber direction. Type 1 collagen (COL-I) expression on 0° scaffolds increased significantly with 10% strain ($p < 0.01$), and remained higher than the free culture (FC) group over 3 h (Fig. 6a, $p < 0.05$). COL-I expression on 30° and 90° scaffolds also increased within 0.5 h after strain ($p < 0.05$), but decreased to baseline levels within 3 h. Lysyl oxidase (LOX) expression on 0° scaffolds increased with strain ($p < 0.05$), and was significantly higher than both 30° and 90° scaffolds within 0.5 h (Fig. 6b, $p < 0.05$).

Tenascin C (TNC) expression increased within 1 h of loading for all orientations, with 0° samples significantly higher than 30° samples ($p < 0.05$). By 3 h expression returned to baseline levels (Fig. 6c).

DISCUSSION

In this work, we examined the translation of macroscopic scaffold deformations to cellular and nuclear deformations for MSCs seeded on directionally biased nanofibrous substrates. These investigations were intended to understand how directional biases in micro-architecture modulate the effects of macroscopically applied tensile deformations. As expected for anisotropic materials, the apparent Poisson's ratio of these scaffolds was direction-dependent, indicating that uniaxial tensile deformations result in different two-dimensional strain fields depending on fiber orientation. Moreover, as nanofiber rotation and strain depend on the direction of their alignment, these findings suggest that not only the magnitude of applied strain, but substrate microstructure as well, must be taken into consideration when examining the mechanobiology of cells on such biomaterials subjected to uniaxial tensile strain. The architectural biases chosen are particularly applicable to the annulus fibrosus of

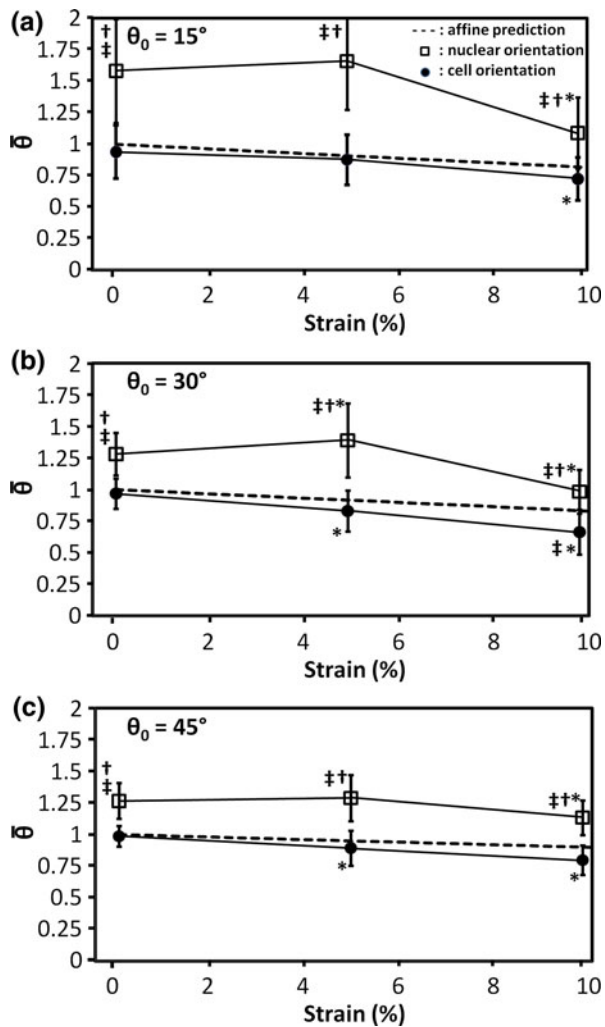


FIGURE 4. Predicted and measured cell and nuclear reorientation as a function of strain for scaffolds oriented at 15° (a), 30° (b), and 45° (c) (dashed line = affine prediction; open square = nuclear orientation; closed circles = cell orientation). θ = angle normalized to initial angle. Data represent the mean \pm SD of $n = 98$ cells/nuclei measured over three different scaffolds for each orientation and strain magnitude (* $p < 0.05$ vs. 0% stretch, † $p < 0.01$ vs. cell orientation, and ‡ $p < 0.05$ vs. affine prediction).

the intervertebral disc, which undergoes tensile deformation in a direction that is not coincident with the primary fiber direction in each lamella. As such, information gathered from this work will help to elucidate the mechanobiologic response of both native tissue and engineered tissue analogues that replicate this complex hierarchy.

Reorientation of MSCs under applied strain varied with initial nanofiber orientation, and in each case, was predicted faithfully with the assumption that reorientation occurs affinely. Conversely, reorientation of MSC nuclei deviated from the affine prediction, as well as from cell body reorientation. While nuclear reorientation was less sensitive to fiber direction, nuclear

deformation was highly sensitive, with NAR exhibiting a scaffold orientation-dependent response to tensile strain. Increases in expression of genes associated with ECM production and crosslinking were greatest and most sustained in cases where the nucleus elongated most. These findings suggest that substrate micro-architecture may anisotropically modulate the bio-synthetic activities of mechanically stimulated MSCs.

Aligned electrospun PCL scaffolds possess orientation-dependent mechanical properties; large reductions in modulus are observed as the direction of strain varies by more than 15° from the prevailing fiber direction (Fig. 2d).²² Large Poisson's ratios (> 1) for 0° , 15° , and 30° scaffolds are likely due to the collapsing of pores as fibers are recruited toward the direction of applied strain, as even in these highly aligned nanofibers there is some degree of dispersion.²⁰ Understanding the dependence of Poisson's ratio on fiber orientation is important in interpreting the physical effects of tensile strain at the macroscopic scale on local deformations at the cellular and sub-cellular scale. For example, a Poisson's ratio greater than 1 indicates that changes in the nuclear aspect ratio are as much, if not more, a consequence of compression in the transverse direction due to squeezing of the cells by the contracting scaffold as it is a consequence of the tensile strains along the loading/fiber direction. A lower Poisson's ratio for 90° scaffolds (~ 0.20) suggests that loading transverse to the fibers may simply pull them apart, without compressing fibers along the transverse direction; this is supported by the low modulus measured for 90° scaffolds, and is consistent with investigations of native fiber reinforced soft tissues.^{18,21}

Poisson's ratio is an important determinant of fiber reorientation, as large lateral contractions lead to increased fiber rotations under uniaxial extension. Previous studies on nanofibrous scaffolds formed from both PCL and PEUU (poly(ester urethane)urea) have shown that local strain fields in electrospun materials can be heterogeneous, and fiber deformations can be complex.^{13,38,39} In this work, we were interested in understanding whether local reorientation of electrospun PCL nanofibers was consistent with the macroscopic applied deformation using resident MSCs as local markers of fiber orientation. Many previous studies have demonstrated that cells elongate on nanofibrous scaffolds and adopt the alignment of the underlying scaffold.^{1,20,26} This is evident in this study as well, both by simple observation (Figs. 2, 3) and by quantification of cell alignment in the undeformed state (Fig. 4). When predictions of cell rotation were computed using measured Poisson's ratios, cell reorientation closely followed the macroscopic deformation, with cells reorienting in an affine manner for each of the fiber orientations examined. These findings show, for

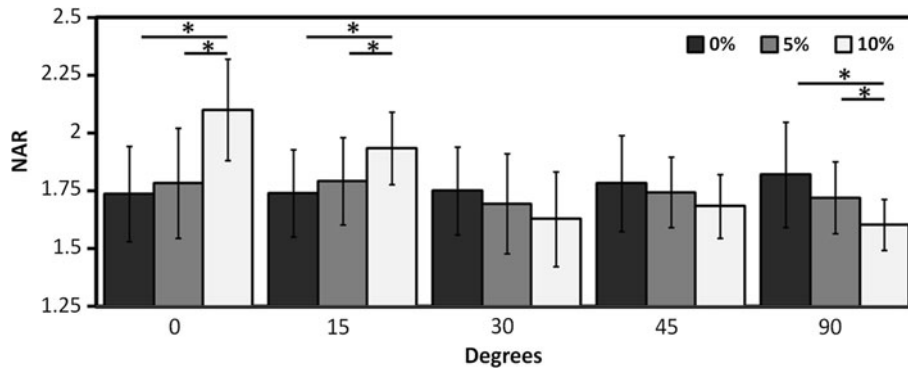


FIGURE 5. Nuclear aspect ratio (NAR) as a function of applied strain and scaffold orientation. The NAR increased with 10% strain on scaffolds with 0° and 15° fiber orientations, but decreased for scaffolds with an orientation of 90° ($*p < 0.05$). No significant changes in NAR were observed on scaffolds with 30° and 45° fiber orientations. Data represent the mean \pm SD of $n = 50$ nuclei measured over three different scaffolds for each orientation and strain magnitude.

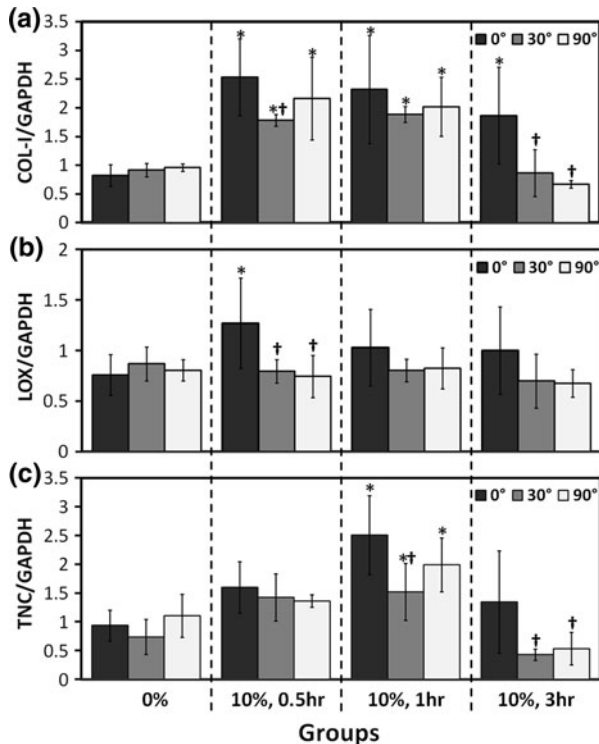


FIGURE 6. Expression of type I collagen (COL-I) (a), lysyl oxidase (LOX) (b), and tenascin C (TNC) (c) normalized to the housekeeping gene (GAPDH) as a function of fiber angle and duration of static tensile stretch ($n = 3$, $*p < 0.05$ vs. 0% stretch and $†p < 0.05$ vs. 0°). Data represent the mean \pm SD.

the first time, that PCL nanofibers deform affinely under uniaxial extension, and that the amount of direct tensile stress experienced (as opposed to shearing as fibers reorient) by cells varies with scaffold alignment. Continuum-based models such as those previously applied to mature nanofiber-based constructs^{4,31,32} may be used to characterize such behaviors.

Interestingly, cell nuclei failed to reorient in an affine manner, suggesting that cellular and subcellular deformations are dissimilar. This is not surprising

given recent measurements of subcellular elements that indicate the nucleus is much stiffer than its surrounding cytoplasm.¹⁰ Moreover, the nucleus is mechanically linked with the cytoplasm through heteromeric protein complexes on the nuclear envelope.⁹ It is unclear how these elements transmit external loads to the nucleus. However, this study suggests that their mechanical role may be quite complex, and that they may even act to resist movement of the nucleus as a cell deforms and/or rotates. We have previously shown that scaffold deformations are transmitted to the nuclei of MSCs on nanofibrous scaffolds primarily through the actin cytoskeleton, while baseline cell and nuclear morphology is in part controlled by microtubules.²⁸ Further work will be necessary to determine what the physical role of these linkages is in inducing elastic deformations and rigid rotations of the nucleus.

Despite reduced reorientation of the nuclear axes, the ratio of their lengths, as measured by the nuclear aspect ratio (NAR) illustrated that scaffold strain was transmitted to the nucleus in each fiber orientation examined. NAR changed with strain, but the manner in which NAR changed was dependent on fiber orientation, suggesting that scaffold anisotropy elicits differential changes in nuclear morphology. For instance, in 0° scaffolds, tensile strain resulted in a significant increase in NAR, indicating elongation of the already elliptical nucleus. While NAR was identical in each scaffold orientation prior to strain, MSCs on 15° scaffolds demonstrated less dramatic changes in NAR with strain compared to 0°. For MSCs on 30°, 45°, and 90° scaffolds, strain decreased NAR, indicating that nuclei became less elliptical (i.e., rounder).

These findings are particularly interesting in the context of recent evidence suggesting that nuclear morphology is an indicator and/or effector of cell phenotype.^{11,40,42} Consistent with this role, application of strain resulted in measurable changes in gene expression, including up-regulation of genes associated

with fibrous tissue formation and maturation. Similar to changes in NAR, application of 10% uniaxial strain yielded differing responses in the degree and duration of gene expression, depending on fiber orientation. COL-I expression was elevated for MSCs each on each orientation examined within 0.5 h of strain and remained elevated at 1 h (Fig. 6a). Interestingly, COL-I expression remained elevated 3 h after strain only for MSCs aligned along the direction of strain (0°), while it returned to baseline levels when cells were either oblique (30°) or perpendicular (90°). We have shown previously that when static strain is applied to MSCs on aligned nanofibrous scaffolds, their nuclei deform initially and then relax back to their original configuration within 2 h.²⁸ It is therefore interesting that changes in COL-I expression were sustained with maximal changes in NAR (on 0° scaffolds), long after the nucleus has returned to its undeformed configuration. Dependence of COL-I on nuclear shape has also been observed previously by modulating MSC nuclear shape through controlled micropatterned adhesive surfaces.⁴⁰ Transience in COL-I expression for MSCs on 30° and 90° scaffolds may suggest that sustained mechanical induction of certain genes requires that a nuclear deformational threshold be exceeded. This is supported by strain-induced changes in LOX and TNC expression as well: LOX expression increased only after 0.5 h strain for 0° scaffolds, and significantly greater strain-induced expression of TNC was observed for MSCs on 0° scaffolds compared to 30° and 90° . These findings are consistent with recent work in which MSCs aligned on elastomeric channels responded to tensile strain differentially depending on the direction of strain.^{17,19} Additionally, because nuclear shape relaxes to its undeformed state after 2 h,²⁸ the expression of genes whose levels decayed back to unstrained levels may be directly dependent on nuclear morphology, while COL-I, which maintained elevated expression levels when strain coincided with the direction of cell alignment, may be stimulated by changes in nuclear shape, but sustained via additional feedback signaling mechanisms. In future work, it will be important to isolate the effects of cell alignment from baseline and time-dependent nuclear deformation in order to decode the mechanosensing machinery that drives physically induced phenotypic shifts in MSCs.

CONCLUSIONS

This study examined the response of MSCs to uniaxial strain on aligned nanofibrous scaffolds. MSC reorientation and changes in nuclear morphology were strongly dependent upon the directionality of nanofibers—and therefore cells—with respect to the loading

axis. This translated to changes in gene expression depending on fiber alignment. These findings demonstrate that macroscopic deformational loading alone cannot be considered when investigating the effects of tensile strain on cell mechanobiology. Instead, an integrative, multi-scale approach that accounts for substrate microstructure and deformation is required. In this way, electrospun scaffolds present a valuable tool for the study of mechanobiology, whereby cell morphology and directionality can be prescribed in order to better understand the translation of externally applied mechanical forces into biomolecular responses. Moving forward, it will be important to map these responses as the scaffolds mature into tissue-like structures with long-term culture. Native tissues, such as the annulus fibrosus and meniscus, develop complex strain profiles at the cell and fiber level, despite relatively uniform macroscopic deformations.^{6,7,41} Moreover, these responses will need to be understood in the context of the dynamic and multi-directional loading environments that scaffolds will be subjected to when placed *in vivo*. Such work will help to further the application of these scaffolds for regenerative medicine applications in soft tissue repair and regeneration.

ACKNOWLEDGMENTS

This work was supported with funding from the National Institutes of Health (R01 EB02425, R01 AR056624), the Penn Center for Musculoskeletal Disorders, and the Human Frontiers in Science Program.

REFERENCES

- ¹Baker, B. M., and R. L. Mauck. The effect of nanofiber alignment on the maturation of engineered meniscus constructs. *Biomaterials* 28(11):1967–1977, 2007.
- ²Baker, B. M., A. S. Nathan, A. O. Gee, and R. L. Mauck. The influence of an aligned nanofibrous topography on human mesenchymal stem cell fibrochondrogenesis. *Biomaterials* 31(24):6190–6200, 2010.
- ³Baker, B. M., A. S. Nathan, G. R. Huffman, and R. L. Mauck. Tissue engineering with meniscus cells derived from surgical debris. *Osteoarthr Cartil* 17(3):336–345, 2009.
- ⁴Baker, B. M., N. L. Nerurkar, J. A. Burdick, D. M. Elliott, and R. L. Mauck. Fabrication and modeling of dynamic multi-polymer nanofibrous scaffold. *J. Biomech. Eng.* 131(10):101012, 2009.
- ⁵Baker, B. M., S. P. Shah, A. H. Huang, and R. L. Mauck. Dynamic tensile loading improves the functional properties of mesenchymal stem cell-laden nanofiber-based fibrocartilage. *Tissue Eng. Part A* 17(9):1–11, 2011.
- ⁶Bruehlmann, S. B., P. A. Hulme, and N. A. Duncan. In situ intercellular mechanics of the bovine outer annulus fibrosus subjected to biaxial strains. *J. Biomech.* 37(2):223–231, 2004.

- ⁷Buehlmann, S. B., J. R. Matyas, and N. A. Duncan. Collagen fibril sliding governs cell mechanics in the annulus fibrosus: an in situ confocal microscopy study of bovine discs. *Spine* 29(23):2612–2620, 2004.
- ⁸Connelly, J. T., A. J. Garcia, and M. E. Levenston. Inhibition of in vitro chondrogenesis in RGD-modified three-dimensional alginate gels. *Biomaterials* 28:1071–1083, 2007.
- ⁹Dahl, K. N., E. A. Booth-Gauthier, B. Ladoux, *et al.* In the middle of it all: mutual mechanical regulation between the nucleus and the cytoskeleton. *J. Biomech.* 43(1):2–8, 2009.
- ¹⁰Dahl, K. N., S. M. Kahn, K. L. Wilson, and D. E. Discher. The nuclear envelope lamina network has elasticity and a compressibility limit suggestive of a molecular shock absorber. *J. Cell Sci.* 117:4779–4786, 2004.
- ¹¹Dahl, K. N., A. J. Ribeiro, and J. Lammerding. Nuclear shape, mechanics, and mechanotransduction. *Circ. Res.* 102(11):1307–1318, 2008.
- ¹²Discher, D. E., D. J. Mooney, and P. W. Zandstra. Growth factors, matrices, and forces combine and control stem cells. *Science* 324:1673–1677, 2009.
- ¹³Driscoll, T. D., N. L. Nerurkar, N. T. Jacobs, D. M. Elliott, and R. L. Mauck. Shear mechanics of electrospun scaffold for annulus fibrosus tissue engineering. *J. Mech. Behav. Biomed. Mater.* (in press).
- ¹⁴Engler, A. J., S. Sen, H. L. Sweeney, and D. E. Discher. Matrix elasticity directs stem cell lineage specification. *Cell* 126(4):677–689, 2006.
- ¹⁵Huang, A. H., M. J. Farrell, M. Kim, and R. L. Mauck. Long-term dynamic loading improves the mechanical properties of chondrogenic mesenchymal stem cell-laden hydrogels. *Eur. Cell. Mater.* 19:72–85, 2010.
- ¹⁶Huang, A. H., A. Stein, and R. L. Mauck. The complex transcriptional topography of mesenchymal stem cell chondrogenesis for cartilage tissue engineering. *Tissue Eng. Part A* 16(9):2699–2708, 2010.
- ¹⁷Kurpinski, K., J. Chu, C. Hashi, and S. Li. Anisotropic mechanosensing by mesenchymal stem cells. *Proc. Natl Acad. Sci. USA* 103(44):16095–16100, 2006.
- ¹⁸Lake, S. P., K. S. Miller, D. M. Elliott, and L. J. Soslowsky. Effect of fiber distribution and realignment on the nonlinear and inhomogeneous mechanical properties of human supraspinatus tendon under longitudinal tensile loading. *J. Orthop. Res.* 27(12):1596–1602, 2009.
- ¹⁹Li, Y., J. S. Chu, K. Kurpinski, X. Li, D. M. Bautista, L. Yang, K. L. Paul Sung, and S. Li. Biophysical regulation of histone acetylation in mesenchymal stem cells. *Biophys. J.* 100(8):1902–1909, 2011.
- ²⁰Li, W. J., R. L. Mauck, J. A. Cooper, X. Yuan, and R. S. Tuan. Engineering controllable anisotropy in electrospun biodegradable nanofibrous scaffolds for musculoskeletal tissue engineering. *J. Biomech.* 40(8):1686–1693, 2007.
- ²¹Lynch, H. A., W. Johannessen, J. P. Wu, A. Jawa, and D. M. Elliott. Effect of fiber orientation and strain-rate on the uniaxial tensile material properties of tendon. *J. Biomech. Eng.* 125:726–731, 2003.
- ²²Marchand, F., and A. M. Ahmed. Investigation of the laminate structure of lumbar disc annulus fibrosus. *Spine* 15:402–410, 1990.
- ²³Mauck, R. L., B. M. Baker, N. L. Nerurkar, J. A. Burdick, W. J. Li, R. S. Tuan, and D. M. Elliott. Engineering on the straight and narrow: the mechanics of nanofibrous assemblies for fiber-reinforced. *Tissue Eng. Part B Rev.* 15:171–193, 2009.
- ²⁴Mauck, R. L., X. Yuan, and R. S. Tuan. Chondrogenic differentiation and functional maturation of bovine mesenchymal stem cells in long-term agarose culture. *Osteoarthritis Cartilage* 14(2):179–189, 2006.
- ²⁵McBeath, R., D. M. Pirone, C. M. Nelson, K. Bhadriraju, and C. S. Chen. Cell shape, cytoskeletal tension, and RhoA regulate stem cell lineage commitment. *Dev. Cell.* 6(4):483–495, 2004.
- ²⁶Moffat, K. L., A. S. Kwei, J. P. Spalazzi, S. B. Doty, W. N. Levine, and H. H. Lu. Novel nanofiber-based scaffold for rotator cuff repair and augmentation. *Tissue Eng. Part A* 15(1):115–126, 2009.
- ²⁷Mow, V. C., and R. Huijskes. Basic Orthopaedic Biomechanics and Mechanobiology. Philadelphia, PA: Lippincott Williams & Wilkins, 1991.
- ²⁸Nathan, A. S., B. M. Baker, N. L. Nerurkar, and R. L. Mauck. Mechano-topographic modulation of stem cell nuclear shape on nanofibrous scaffolds. *Acta Biomater.* 7(1):57–66, 2011.
- ²⁹Nerurkar, N. L., B. M. Baker, S. Sen, E. E. Wible, D. M. Elliott, and R. L. Mauck. Nanofibrous biologic laminates replicate the form and function of the annulus fibrosus. *Nat. Mater.* 8(12):986–992, 2009.
- ³⁰Nerurkar, N. L., D. M. Elliott, and R. L. Mauck. Mechanics of oriented electrospun nanofibrous scaffolds for annulus fibrosus tissue engineering. *J. Orthop. Res.* 25(8):1018–1028, 2007.
- ³¹Nerurkar, N. L., R. L. Mauck, and D. M. Elliott. ISSLS prize winner: integrating theoretical and experimental methods for functional tissue engineering of the annulus fibrosus. *Spine* 33(25):2691–2701, 2008.
- ³²Nerurkar, N. L., R. L. Mauck, and D. M. Elliott. Modeling interlamellar interactions in angle-ply biologic laminates for annulus fibrosus tissue engineering. *Biomech. Model. Mechanobiol.* doi:10.1007/s10237-011-0288-0, 2011.
- ³³Nerurkar, N. L., S. Sen, A. H. Huang, D. M. Elliott, and R. L. Mauck. Engineered disc-like angle-ply structures for intervertebral disc replacement. *Spine* 35(8):867–873, 2010.
- ³⁴Nesti, L. J., W. J. Li, R. M. Shanti, Y. J. Jiang, W. Jackson, B. A. Freedman, T. R. Kuklo, J. R. Giuliani, and R. S. Tuan. Intervertebral disc tissue engineering using a novel hyaluronic acid-nanofibrous scaffold (HANFS) amalgam. *Tissue Eng. Part A* 14(9):1527–1537, 2008.
- ³⁵Peltz, C. D., S. M. Perry, C. L. Getz, and L. J. Soslowsky. Mechanical properties of the long-head of the biceps tendon are altered in the presence of rotator cuff tears in a rat model. *J. Orthop. Res.* 27(3):416–420, 2009.
- ³⁶Petrie, T. A., J. E. Raynor, D. W. Dumbauld, T. T. Lee, S. Jagtap, K. L. Templeman, D. M. Collard, and A. J. Garcia. Multivalent integrin-specific ligands enhance tissue healing and biomaterial integration. *Sci. Transl. Med.* 2(45):45ra60, 2010.
- ³⁷Pittenger, M. F., A. M. Mackay, S. C. Beck, R. K. Jaiswal, R. Douglas, J. D. Mosca, M. A. Moorman, D. W. Simonetti, S. Craig, and D. R. Marshak. Multilineage potential of adult human mesenchymal stem cells. *Science* 284(5411):143–147, 1999.
- ³⁸Stella, J. A., J. Liao, Y. Hong, W. David Merryman, W. R. Wagner, and M. S. Sacks. Tissue-to-cellular level deformation coupling in cell-microintegrated elastomeric scaffolds. *Biomaterials* 29(22):3228–3236, 2008.
- ³⁹Stella, J. A., W. R. Wagner, and M. S. Sacks. Scale-dependent fiber kinematics of elastomeric electrospun scaffolds for soft tissue engineering. *J. Biomed. Mater. Res. A* 93(3):1032–1042, 2010.
- ⁴⁰Thomas, C. H., J. H. Collier, C. S. Sfeir, and K. E. Healy. Engineering gene expression and protein synthesis by

- modulation of nuclear shape. *Proc. Natl Acad. Sci. USA* 99(4):1972–1977, 2002.
- ⁴¹Upton, M. L., C. L. Gilchrist, F. Guilak, and L. A. Setton. Transfer of macroscale tissue strain to microscale cell regions in the deformed meniscus. *Biophys. J.* 95(4):2116–2124, 2008.
- ⁴²Webster, M., K. L. Witkin, and O. Cohen-Fix. Sizing up the nucleus: nuclear shape, size and nuclear envelope assembly. *J. Cell Sci.* 122:1970–1978, 2009.
- ⁴³Xie, J., X. Li, J. Lipner, C. N. Manning, A. G. Schwartz, S. Thomopoulos, and Y. Xia. “Aligned-to-random” nanofiber scaffolds for mimicking the structure of the tendon-to-bone insertion site. *Nanoscale* 2(6):923–926, 2010.
- ⁴⁴Yang, L., R. A. Kandel, G. Chang, and J. P. Santerre. Polar surface chemistry of nanofibrous polyurethane scaffold affects annulus fibrosus cell attachment and early matrix accumulation. *J. Biomed. Mater. Res. A* 91(4):1089–1099, 2009.